Doctoral Dissertation

GSTA4 governs melanoma cell resistance to anti-tumor immunity

GSTA4 はメラノーマ細胞の抗腫瘍免疫応答に対する抵抗性を制御する

Ucche Sisca

Section of Host Defences
Institute of Natural Medicine
Graduate School of Medicine and Pharmaceutical Sciences
University of Toyama

2023

Contents

Preface

This thesis has been submitted to the Affiliation of Graduate School of Medicine and Pharmaceutical Sciences for Education, University of Toyama, Japan, for the degree of Doctor of Philosophy Ph. D This research was conducted at the Institute of Natural Medicine's Laboratory of Cancer Biology and Immunology, Section of Host Defenses.

The findings of this thesis were published in two papers, which are listed below:

1. Mojic, M., Shitaoka, K., Ohshima, C., Ucche, S., Lyu, F., Hamana, H., Tahara, H., Kishi, H., & Hayakawa, Y. (2021). NKG2D defines tumor-reacting effector CD8$^+$ T cells within tumor microenvironment. *Cancer science, 112*(9), 3484–3490.

2. Ucche, S., Yokoyama, S., Mojic, M., Oki, K., Ohshima, C., Tsuihiji, H., Takasaki, I., Tahara, H., & Hayakawa, Y. (2023). GSTA4 governs melanoma immune resistance and metastasis. *Molecular cancer research : MCR, 21*(1), 76–85.

Abstract

Cancer immunotherapy, such as immune checkpoint blockade (ICB), has been successful for many types of cancer including melanoma; however, unresponsiveness to ICB remains as a major obstacle to realizing further clinical benefit. While the primary immune resistance of cancer cells might be caused by their low immunogenicity and/or expression of immune-suppressive phenotypes, an acquired immune resistance mechanism against cancer immune therapy has not been well understood. Among factors involved in cancer cells escaping from immune responses, an intrinsic defect in the IFN-γ response is considered as one of the major players allowing cancer cells to evade host immunity. In this study, I aim to understand an acquired resistance mechanism of melanoma cells to antigen-specific anti-tumor immunity.

Firstly, to understand the immunological status of tumor antigen-specific CD8^{+} T cells in the tumor microenvironment during tumor progression, we established a bioluminescence imaging model to monitor the interplay between occult immunogenic tumor and host anti-tumor immunity. Using mouse B16 melanoma cells expressing ovalbumin (OVA) and luciferase (B16OVA-Luc2 cells), we monitored the status of B16OVA-Luc2 melanoma cells in mice immunized with a model tumor antigen ovalbumin (OVA). We found that the cell growth was biphasic during tumor progression: initial progression, suppressed by a CD8^{+} T cell-dependent immune response, and thereafter showed secondary progression by escaping from host immunity in OVA-immunized mice.

We next generated cell lines after *in vivo* passage through distinct immunological conditions. B16OVA-Luc2 tumors exposed to OVA-specific CD8^{+} T cell immunity in OVA-immunized B6 mice were isolated, and we established five variants (IMM1, 2, 5, 6, and 8 cell lines). For comparison, B16OVA-Luc2 tumors from non-immunized naïve B6 mice or OVA-immunized IFN-γ-deficient mice were also isolated, and we established four variants, namely NIMM (1, 3, 4, 5) cell lines or GKO-IMM (1, 2, 3, 4) cell lines, respectively. To test the capacity of those different variants for immunogenicity, those cell lines were re-challenged

in OVA-immunized B6 mice. In contrast to NIMM and GKO-IMM cell lines, IMM cell lines showed progressive growth in OVA-immunized mice upon re-challenge and specifically lost their OVA antigen expression. Furthermore, we found that IMM cell lines gained resistance to the IFN-γ-induced oxidative stress response. By subjecting those different cell lines to DNA microarray analysis, we found the expression of glutathione-S-transferase alpha 4 (*Gsta4*) was highly up-regulated in the IMM cells compared to the parental or other control (NIMM or GKO-IMM) cell lines. To further determine the functional role of *Gsta4* in protecting the IMM cells from oxidative stress, we established the B16OVA cell line overexpressing *Gsta4* (GSTA4 OE) or IMM cell line knocking down *Gsta4* (shGSTA4). GSTA OE cell lines showed resistance to the IFN-γ-induced-oxidative stress. In addition, shGSTA4 cell lines showed to be sensitive to IFN-γ-induced oxidative stress responses. In addition, the growth of GSTA4 OE cells was more aggressive than that of parental B16OVA cells in the OVA-immunized B6 mice. Furthermore, shGSTA4 cells reinvigorated the responsiveness to anti-PD-1 treatment *in vivo*. Importantly, melanoma patients with low *GSTA4* expression were better responders and showed better progression-free survival rates to anti-PD-1 therapy.

Collectively, these studies show how to identify the immunological status of tumor antigen-specific CD8$^+$ T cells in the tumor microenvironment during tumor progression and highlight a novel mechanism whereby cancer cells escape from host immunity by acquiring resistance to oxidative stress responses through the upregulation of *Gsta4*.

1. Introduction

Cancer is a disease where normal cells grow abnormally without control and potentially invade other body parts (1). It was known that cancer shares six distinct main hallmarks; 1. sustaining proliferative signaling, 2. evading growth suppressors, 3. activating invasion and metastasis, 4. enabling replicative immortality, 5. inducing angiogenesis, and 6. resisting cell death (2). Moreover, it is now appreciated that avoiding immune destruction is one of the characteristics of cancer cells (3), indicating the ability of cancer cells to evade the immune system response to maintain its proliferation capacity.

The interplay between cancer and immune cells is complex and has been debated extensively. It was first hypothesized under the cancer immunosurveillance concept that the immune system can recognize and eradicate the growth of cancer cells before clinically detected (4–6). However, apart from the importance of eliminating cancer cells, there is growing evidence that immunity not only eliminates the tumor cells but also sculpts the immunogenic phenotype of tumors to evade the immune control (7). This process is called cancer immunoediting and consists of three phases: elimination, equilibrium, and escape. The immune system recognizes and destroys cancer cells in the elimination phase, which refers to the immunosurveillance concept. Some of the cancer cells might not be entirely eliminated and thus enter the equilibrium phase where it will be maintained with the immune system. However, due to the constant and high immune pressure, the immune system shapes the cancer cells to generate new tumor variants that can be detected in the escape

phase (8). There are many known mechanisms of how cancer cells escape from immunity, and one of the mechanisms is the defect of the interferon-γ (IFN-γ) signaling pathway (9,10).

IFN-γ is the lone member of type II interferon (11). It is produced mainly by natural killer (NK) cells and natural killer T (NKT) cells in the innate immune system, and a subset of CD4$^+$ T cells and CD8$^+$ T cells are the producers in the adaptive immune system (12). IFN-γ regulates its effector function by engaging with the IFN-γ receptor (IFN-γR) and activated the downstream receptor-associated Janus kinase, JAK 1 and JAK 2. The phosphorylation of JAK 1/2 will activate the signal transducer and activator of transcription-1 (STAT-1), which then form a complex and bind to the interferon-γ activated sequence (GAS) to induce the transcription of various genes (13–15). The activation of IFN-γ plays crucial role in the host defense and immune regulation and the importance of IFN-γ in eradicating tumor cells has been long-term appreciated (16). The first indication to show that IFN-γ is important for generating antitumor immune response was done by showing the rejection of tumor growth in the presence of neutralizing monoclonal antibodies specific for IFN-γ in the Meth A-fibrosarcoma tumor model (17). In addition, mice lacking the IFN-γ receptor and/or the STAT1 were shown to be more sensitive to methylcoanthrene-induced carcinogenesis. The experiment was supported by discovering that melanoma and lung melanoma adenocarcinoma cell lines had inactivating mutations in the IFN-γ pathway, suggesting that cancer cells might avoid the cancer surveillance by becoming insensitive to IFN-γ (18). The effect of IFN-γ have been found to

stimulate the expression of MHC class I genes, which increases tumor immunogenicity and makes the tumor cells more sensitive to tumor recognition and destruction (19–22). IFN-γ also known to exhibit direct antitumor effect by inducing tumor cell cycle arrest by enhancing the expression of cell cycle inhibitor proteins p27Kip, p16, or p21 (23–25). Moreover, IFN-γ also found to stimulate mitochondria-derived reactive oxygen species (mROS) which inducing autophagy-associated apoptosis that is dependent on the activation cytosolic phospholipase A2 (26). Furthermore, it has been reported that IFN-γ induces cellular senescence in cancer cells by enhancing the reactive oxygen species (ROS) and DNA damage response (27). In addition, a recent study demonstrated that IFN-γ released from CD8^{+} T cells promotes tumor cell lipid peroxidation and induces ferroptosis, an oxidative stress-related programmed cell death (28). Taken together, the above evidence suggests the importance of IFN-γ in the mediated antitumor immune response.

On the other hand, it was discovered that IFN-γ also contributed to the growth and progression of tumor cells. It is reported that IFN-γ has the capacity to induce carcinogenesis and metastasis through inducing inflammatory responses and immunosuppression mechanisms (29–31). IFN-γ signaling has been reported to induce melanocyte activation and mediates the pro-tumorigenic effect of UVB-induced melanoma cells, where those effect was abolished by the use of IFN-γ blocking antibody (32). Furthermore, IFN-γ signaling is reported to induce PD-L1 expression in tumor cells, which is one of the escape strategies of cancer cells from immunity (33). The increase of PD-L1 expression has been

reported to the resistance to NK cell killing activity, while the blocking of IFN-γ signaling leads to an increase in the lysis capacity of NK cells (34). IFN-γ has been known to select tumor cells through constant immune pressure, which leads to the escape of tumor cells from immunity and those escaped cells have been found to lose antigen expression (35). It was shown that IFN-γ promotes tumor escape in the colon carcinoma mouse model by downregulating the endogenous antigen gp70, correlated with an increased tumor incidence in mice (36). In addition to IFN-γ-induced antigen loss, IFN-γ-treated melanoma cells was reported to have a loss of the Melan-A and gp100 antigen, which enable the tumor cells to evade the cytotoxic-T-lymphocytes (CTL) (37). In this regard, we also recently reported that antigen-specific immunity by CTL and IFN-γ increases genomic instability to select cancer cells for evading immunity. We observed copy-number alterations (CNA) related to DNA damage response and modulation of DNA repair gene as a consequence of *in vivo* exposure of tumors expressing immunogenic antigen to CTL-producing-IFN-γ. This was not only due in part to the loss of tumor-antigen but also accumulated during immunological selection, thereby contributing to intra-tumor heterogeneity (38).

In this study, we investigated how tumor cells escape from the IFN-γ-dependent immune response through the immunoediting process by analyzing originally established immune-escape variants of melanoma cells. We found that the immune-escape melanoma variants gained resistance to the IFN-γ-induced oxidative stress response, and glutathione-S-transferase-4 (GSTA4) was a critical molecule in this process. Considering the importance of GSTA4 in

controlling the IFN-γ responsiveness, our results highlight a novel mechanism whereby cancer cells escape from host immunity by acquiring resistance to oxidative stress responses through the upregulation of *Gsta4*.

2. Materials and Methods

Reagents

4-hydroxynonenal (4-HNE) was purchased from EMD MIlipore (#393204; Darmstadt, Germany). IFN-γ was purchased from Pepro Tech (Rocky Hills, NJ, USA). *Gsta4* and *β-actin* primers were purchased from Invitrogen (Carlsbad, CA, USA). An antibody against GSTA4 was obtained from EMD Millipore (#ABS1652, Darmstadt, Germany), an antibody against Flag-tag was obtained from Sigma-Aldrich (#F1804, Saint Louis, MO, USA), and an antibody against β-actin was obtained from Santa Cruz Biotechnology (#sc-47778; Santa Cruz, CA, USA). WST-8 was purchased from Nacalai Tesque (#07553-44; Kyoto, Japan). Cell ROX^{TM} Deep Red Flow Cytometry Assay kit was purchased from Invitrogen (#C10491; Carlsbad, CA, USA). Pgl4.50 [luc2P/CMV-RE-Hygro] vector and D-luciferin were obtained from Promega (Sunnyvale, CA, USA). Lipofectamine 2000 was purchased from Invitrogen (Carlsbad, CA, USA). Hygromycin B was obtained from Nacalai Tesque (Kyoto, Japan).

Cells

The murine B16 melanoma cell line expressing ovalbumin (MO4:B16OVA) was kindly provided by Dr. Shinichiro Fujii (RIKEN). To establish B16OVA cells stably expressing luciferase (B16OVA-Luc2), B16OVA cells were transfected with a pGL4.50 vector and cloned by limiting dilution as described previously (39). Malme3M, UACC62 (obtained from National Cancer Institute), and MeWo

(obtained from American Type Culture Collection) were cultured in RPMI1640 (Nissui, Japan). The media were supplemented with 2 mM L-glutamine, 10% fetal bovine serum, 100 U/mL penicillin, and 100 μg/mL streptomycin. The cells were maintained at 37°C in a humidified atmosphere with 5% CO_2.

Mice

Six to eight-week-old wild-type C57BL/6J (WT) mice were purchased from Japan SLC, Inc. (Hamamatsu, Japan). IFN-$\gamma^{-/-}$ (IFN-γ-KO) mice were kindly provided by Dr. Y. Iwakura (Tokyo University of Science, Chiba, Japan) and maintained at Laboratory Animal Research Center, Institute of Medical Science, University of Tokyo. All experiments were approved (A2016INM-9, A2019INM-4) and performed according to the Care and Use of Laboratory Animals of the University of Toyama guidelines and the Animal Care and Use Committee of the Insitute of Medical Science of the University of Tokyo.

Bioluminescence imaging of in vivo cancer cell growth

Mice were inoculated subcutaneously (sc) with B16OVA-Luc2 cells and tumor growth was monitored by bioluminescence imaging. To obtain bioluminescence images, mice were injected with D-luciferin (Promega, 150 mg/kg, i.p), and luminescence was measured with an *in vivo* imaging system (IVIS Lumina II, Perkin Elmer, MA, USA) 20 min after the D-luciferin injection. Regions of interest analyses were performed using Living Image 4.2 Software (Caliper Life Science, Hopkinton, MA, USA) to determine the light emitted from the tumor. For each

mouse, all values were determined as photons per sec (photon/sec). The group of mice received sc injections of 100 μg of chicken ovalbumin protein (OVA, Sigma) emulsified in complete Freund's adjuvant (CFA, Sigma) or incomplete Freund's adjuvant (IFA, Sigma) 14 d (OVA-CFA) or 7 d (OVA-IFA) before tumor inoculation. In some experiments, mice were treated with ip injections of 250 μg of anti- IFN-γ (clone H-22, Bio X Cell), anti-CD8 (clone 53.6.2, Bio X Cell), or anti-NKG2D (clone HMG2D, Bio X Cell).

Establishment of immune-escape variants of B16OVA cells

To prepare cells with different *in vivo* immunological experiences, B16OVA-Luc2 cells (10^5) were used to subcutaneously (s.c) inoculate to WT untreated, WT vaccinated, or IFN-γ-KO vaccinated mice. Twelve (untreated WT or IFN-γ-KO vaccinated mice) or 19 (vaccinated WT mice) days after inoculation, approximately same-sized tumors (~400 mm^3) were aseptically harvested, dissected, and digested with 2 mg/mL collagenase (Roche Diagnostics GmbH) and 0.1 mg/mL DNase I (Roche Diagnostics GmbH) in serum-free RPMI 1640 for 1 h at 37°C. Isolated tumor cells were named 'NIMM' if prepared from tumors from WT untreated mouse, 'IMM' if prepared from WT vaccinated mouse tumors, and 'GKO-IMM' if prepared from IFN-γ-KO vaccinated mouse tumors. All newly established cell lines were cultured *in vitro* for at least 3 weeks before *in vivo* characterization.

Establishment of Gsta4 overexpresses cell lines

To establish the overexpressed cells, we first subcloned the flag-tagged mouse *Gsta4* sequence, synthesized by Thermo Fisher Scientific (Massachusetts, USA), into the pENTR1A vector. The flag- *Gsta4* subcloned into pENTR1A, which was enzymatically cut by restriction enzyme; BamHI and NotI, using polymerase chain reaction (PCR) with PrimeSTAR® HS DNA Polymerase (Takara, Kyoto, Japan). The PCR reaction conditions were 98°C for 10 seconds, 57°C for 15 seconds, 72°C for 1 minute, and 40 cycles. The PCR products were confirmed by gel electrophoresis. The detected band in the agarose gel was cut out and purified by QIAquick Gel Extraction Kit (Qiagen, Hilden, Germany) according to the manufacturer's protocol. The PCR products were assembled using NEBuilder HiFi DNA Assembly (New England BioLabs, Ipswich, MA) at 50°C for 15 minutes. Then, the plasmid was transformed into *E. coli*, and the selected colonies were picked up and cultured in LB with ampicillin at 37°C, 200 rpm, overnight. Next, plasmids were extracted using Nucleospin® Plasmid QuickPure (Takara, Kyoto, Japan) according to the manufacturer's protocol. Plasmids were then verified with the restriction enzyme, PstI, and underwent sequencing analysis.

The m*Gsta4* fragment was then subcloned into pLenti CMV Hygro DEST vector (w117-1), which was a gift from Dr. Campeau E. and Dr. Kaufman P. (Addgene plasmid #17454) (40), by Gateway™ LR Clonase™ II Enzyme mix (Thermo Fisher Scientific, Massachusetts, USA). The plasmids were transformed into *E. coli*, and the selected colonies were picked up and cultured in LB with ampicillin at 37°C, 200 rpm, overnight. Next, plasmids were extracted using Nucleospin® Plasmid QuickPure (Takara, Kyoto, Japan) according to the

manufacturer's protocol. After large-scale amplification, plasmids were prepared using HiSpeed® Plasmid Midi Kit (Qiagen, Hilden, Germany) according to the manufacturer's protocol.

Lentivirus particles were produced as described previously (41). The prepared pLCMVh_mGSTA4 pMD2.G, psPAX2 was transfected into Lenti-X 293T cells (Takara, Kyoto, Japan). The amount of virus was titrated for near quantitative infection with <5% toxicity of non-template virus. For lentiviral delivery, 10^5 cells were plated on Day 1 in 6-well plates, infected to B16OVA on the following day, and cells were selected in 1 μg/mL puromycin.

Establishment of Gsta4 knockdown cell lines

The shRNAs targeting mouse *Gsta4* (TRCN0000103430, TRCN0000103431, TRCN0000103432, TRCN0000103433, and TRCN0000103434) or luciferase were purchased from Dharmacon (Colorado, USA).

The shRNA plasmids with pMD2.G and psPAX2 were transfected into Lenti-X 293T cells (Takara, Kyoto, Japan). Lentivirus particles were produced as described previously (41). The amount of virus was titrated for near quantitative infection with <5% toxicity of non-template virus. For lentiviral delivery, 10^5 cells were plated on Day 1 in 6-well plates, infected to B16OVA on the following day, and cells were selected in 1 μg/mL puromycin.

DNA microarray analysis

Total RNA was extracted from cells using the RNeasy Mini kit (Qiagen, Valencia, CA). Gene expression was analyzed using a GeneChip® system with GeneChip™ Mouse Gene 2.0 ST Array (Affymetrix, Santa Clara, CA, USA), as described

previously (42). In this study, a total of four arrays were used: one for parent cells and three for IMM cells (IMM 1, 2, and 8). Comparison of gene expression levels was conducted using Transcriptome Analysis Console software (Thermo Fisher Scientific, Massachusetts, USA). The microarray dataset was deposited to Gene Expression Omnibus (GEO) with accession number GSE199573. The top 10 and bottom 10 genes were picked up for Figure 9 based on their fold change values.

Cell viability assay

Cells were seeded at a final concentration of 5 x 10^3 cells/well (24 h) or 10^3 cells/well (72 h) in a 96-well plate. After 4 h incubation, cells were treated with 4-HNE for 24 h or IFN-γ for 72 h (37°C, 5% CO_2). After treatment, 10 μL of WST-8 reagent was added and incubated for another 2 h. The absorbance was measured in a microplate reader at 450/620 nm. Cell viability was determined from the absorbance of soluble formazan dye generated by the living cells.

Quantitative polymerase chain reaction (qPCR)

Cells were seeded at a final concentration of 10^5 cells/well in 6-well plates for 48 h and incubated in a humidified atmosphere (37°C, 5% CO_2). Total RNAs were prepared using the RNeasy Plus Mini kit (Qiagen, Hilden, Germany). Expression of *Gsta4* was quantitatively determined by real-time PCR using an ABI Prism 7300 sequence detection system (Life Technologies Corporation, Carlsbad, CA, USA). The expression level of *Gsta4* mRNA was normalized to the β-*actin* gene. The primers used were: 5'-TGA TTG CCG TGG CTC CAT TTA-3' (forward) and 5'-CAA CGA GAA AAG CCT CTC CGT-3' (reverse) for *Gsta4* mRNA and 5'-GGC

TGT ATT CCC CTC CAT CG-3' (forward) and 5'-CCA GTT GGT AAC AAT GCC ATG T-3' (reverse) for *β-actin* mRNA. The expression level of antigen (*Ova*, *gp100*, *Trp1*, *Trp2*, *Mart1*) mRNA was normalized to the *Gapdh* gene. The primers used were: 5'-CCT TGA GCA GCT TGA GAG TATA A-3' (forward) and 5'-CCA TCT TCA TGC GAG GTA AGT-3' (reverse) for *Ova* mRNA, 5'-AGC ACC TGG AAC CAC ATC TA-3' (forward) and 5'-GTT CCA GAG GGC TGT GTA GT-3' (reverse) for *gp100* mRNA, 5'-TGG GGA TGT GGA TTT CTC TC-3' (forward) and 5'-AGG GAG AAA GAA GGC TCC TG-3' (reverse) for *Trp1* mRNA, 5'-AGG TAC CAT CTG TTG TGG CTG GAA-3' (forward) and 5'-AGT TCC GAC TAA TCA GCG TTG GGT-3' (reverse) for *Trp2* mRNA, 5'-ATT GCT CTG CTT ATC GGC TGC T-3' (forward) and 5'-CAC CAT TCC TCC AAT ATC CCT CT-3' (reverse) for *Mart1* mRNA, 5'-AAA TGG TGA AGG TCG GTG TG-3' (forward) and 5'-TGA AGG GGT CGT TAG ATG C-3' (reverse) for *Gapdh* mRNA.

Western blotting

Cells were grown at a final concentration of 10^5 cells/well in 6-well plates for 48 h and incubated in a humidified atmosphere (37°C, 5% CO_2). Cells were collected, washed with PBS, and lysed in lysis buffer (1 M DTT, 1 M sodium orthovanadate, 1 M β-glycerophosphate, 10 mg/mL aprotinin, 10 mg/mL leupeptin, 0.1 M PMSF). The cell lysates were separated by 10% SDS-PAGE and transferred to PVDF membranes. After blocking with 0.1% Tween® 20 in PBS-5% BSA for 1.5 h at room temperature, the membranes were incubated overnight with primary antibodies and then for 1 h with the secondary antibodies. Primary antibodies

were used at a dilution of 1:1000. Secondary antibodies were used at a dilution of 1:2000 and visualized with an enhanced chemiluminescence system.

ROS measurement

Cells were seeded at a final concentration of 5×10^4 cells/well in 6-well plate. After 4-h incubation, cells were treated with IFN-γ 20 U/mL for 72 h and incubated in a humidified atmosphere (37°C, 5% CO_2). In brief, the cells were harvested and stained with CellROX™ Deep Red reagent or medium for the unstained cells. After that, cells were incubated for another 1 h in a humidified atmosphere (37°C, 5% CO_2). Flow cytometric analysis was performed using FACSCanto II (BD Biosciences). FlowJo ver. 10 software (Tree Star, Ashland, OR, USA) was used to quantify intracellular oxidative stress.

Flow cytometry

For characterizing melanoma in response to IFN-γ, cells were seeded at a final concentration of 10^5 in a 6-well plate. After 4 h incubation, cells were treated with IFN-γ 20 U/mL for 48 h and incubated in a humidified atmosphere (37˚C, 5% CO_2). The cells were stained with antibodies against MHC Class I (28-14-8, eBioscience) and CD274/PDL1 (MIH5, eBioscience). For the analysis of tumor-infiltrating lymphocytes, after 14 days of transplantation, tumor samples were prepared as previously described (43). After incubating the cells with anti-CD16/32 (2.4G2), the cells were then incubated with antibodies against CD3 (17A2), CD4 (GK1.5), and CD8α(2.43). Flow cytometry was performed with

FACSCanto II (BD Biosciences) and data were analyzed with FlowJo ver. 10 software (Tree Star, Ashland, OR, USA).

In vivo tumor model

For the subcutaneous tumor model, cells were injected subcutaneously (s.c., 10^5) and tumor growth was assessed by measuring the tumor diameter every two days. In some experiments, the group of mice received s.c injections of 100 μg of chicken ovalbumin protein (OVA, Sigma) emulsified in complete (CFA, Sigma) or incomplete (IFA, Sigma) Freund's adjuvant 14 (OVA-CFA) or 7 (OVA-IFA) days prior to tumor inoculation. In some experiments, anti-PD-1 antibody (RMP1-14, 250 μg/mouse, BioXCell) was administered intraperitoneally on Days 3, 6, and 9 after tumor inoculation. The tumor volume was calculated by the formula (major axis) x (minor axis)^2 x 0.52. Mice with no confirmed tumor were excluded from the data.

Statistical analysis

All the data are expressed as the mean ± SEM and represent at least two independent experiments unless otherwise stated. The groups of 5-10 mice were used to perform all *in vivo* experiments. Significance was analyzed using Student's t-test for comparisons between 2 groups. One-way analysis of variance (ANOVA) with Bonferroni correction was used to compare 3 or more groups. $p < 0.05$ was considered significant.

Data availability

The microarray dataset was deposited to Gene Expression Omnibus (GEO) with accession number GSE199573. The GSTA4 expression in human melanoma in this study was obtained from Cancer Cell Line Encyclopedia. The human melanoma response to anti-PD-1 treatment in correlation with GSTA4 expression is publicly available in the ROC plotter database. The human melanoma survival rates data in response to anti-PD-1 therapy are publicly available in the KM plotter database.

3. Results

3.1. Establishment of immune-escape variants of B16OVA cells

To establish cancer cells escaping from host immunity, we created a murine B16 melanoma cell line expressing ovalbumin (B16OVA) and used it to inoculate to mice immunized with OVA. To precisely monitor the immune control phase of tumor growth by antigen-specific T cells, we first developed a bioluminescence imaging model under different immunological conditions. We use murine B16 melanoma cells expressing ovalbumin (OVA) as a model tumor antigen and firefly luciferase gene to enable tumor growth monitoring by bioluminescence imaging (B16OVA-Luc2 cells). Thus, we implanted the cells in wild-type B6 mice (control), or B6 mice vaccinated with OVA to introduce antigen-specific immune response. By monitoring the luminescence expression of B16OVA-Luc2 cells, we found that the tumor cells grow progressively in the control B6 mice. However, in the OVA-vaccinated B6 mice, the growth of the B16OVA-Luc2 cells showed biphasic increase where it showed initial progression on days 2 to 8, then regressed by the immune control on days 10 to 12, and then showed subsequent lethal progression by escaping from host immunity (Fig. 1).

We found that such biphasic growth might be controlled by CD8$^+$ T cells and host IFN-γ production because it was compromised in OVA-vaccinated WT mice treated with IFN-γ-blocking antibody (Fig. 2) or OVA-vaccinated WT mice treated with a depleting anti-CD8 antibody (Fig. 3). These results strongly indicated that the biphasic *in vivo* growth of B16OVA-

Luc2 tumors in OVA vaccinated mice was controlled by IFN-γ and CD8$^+$ T-cell-dependent anti-tumor immune responses.

Using this model, we then established cell lines after *in vivo* passage through distinct immunological conditions (Fig. 4A). B16OVA tumors exposed to OVA-specific CD8$^+$ T cell immunity in OVA-immunized B6 mice were isolated, and we established five variants of cell lines (IMM 1, 2, 5, 6, and 8). As a comparison, we isolated B16OVA tumors from non-immunized naïve B6 mice or OVA-immunized IFN-γ-knock-out mice were also isolated, and we generated four variants, namely NIMM (1, 3, 4, and 5) cell lines or GKO-IMM (1, 2, 3, and 4) cell lines, respectively. To test the ability of those distinguished variants to provoke tumor antigen-specific immunity, we re-challenged IMM, NIMM, or GKO-IMM cell lines in OVA-immunized B6 mice. We discovered that IMM cell lines showed progressive growth in OVA-immunized mice upon re-challenge, but this phenomenon could not be seen in NIMM and GKO-IMM cell lines. Furthermore, IMM cell lines, but not NIMM and GKO-IMM cell lines, specifically lost their OVA antigen expression but not for the other melanoma antigens (Fig. 5). These results suggest that IMM cell lines acquire the ability to evade the OVA-specific anti-tumor immune response.

3.2. Immune-escape melanoma variants resistant to IFN-γ-induced cytostatic effect and ROS production

IFN-γ is a critical effector molecule of tumor antigen-specific CD8$^+$ T cells, and cancer cells often escape from anti-tumor immunity by losing their

responsiveness to IFN-γ (44). Therefore, we next examined the response of IMM variants to IFN-γ *in vitro*. IFN-γ treatment for 72 h showed a dose-dependent cytostatic effect in parental B16OVA, NIMM3, or GKO-IMM1 cells; however, IMM2 showed significant resistance to *in vitro* IFN-γ treatment together with the capacity to escape the OVA-specific anti-tumor immune response *in vivo* (Fig. 6A). In addition, we confirmed that resistance to IFN-γ treatment in all IMM cell lines, but not in NIMM or GKO-IMM cell lines (Fig. 6B). Importantly, IMM cell lines responded to *in vitro* IFN-γ treatment by upregulating their expression of MHC class I (H-2K^d) or PD-L1 (Fig. 7); therefore, such resistance to IFN-γ -induced cytostatic effect is not due to the lack of their responsiveness to IFN-γ. These results suggest that the ability of IMM cell lines to escape from anti-tumor immunity could result from acquiring resistance to the IFN-γ-induced cytostatic effect and not a loss of IFN-γ-dependent signaling.

It has been reported that IFN-γ induces reactive oxygen species (ROS) and subsequent oxidative stress response to exert its cytostatic effect (27); then, we examined the oxidative stress response in IMM cell lines upon IFN-γ-treatment. In parental B16OVA cells, IFN-γ treatment induced ROS production, whereas IFN-γ-induced ROS production was weak in IMM cell lines (Fig. 8). Therefore, we conclude that immune-resistant melanoma cell variants did not respond to the IFN-γ-induced cytostatic effect due to acquiring resistance to the IFN-γ-induced oxidative stress response.

3.3. Functional upregulation of *Gsta4* in immune-resistant melanoma variants

To comprehend the molecular mechanism by which IMM cell lines acquire resistance to the IFN-γ-induced oxidative stress response, we performed a comprehensive DNA microarray analysis of the gene expression of those cell lines. Amongst the gene upregulated in IMM cell lines compared with the parental B16OVA cells, the most upregulated gene in IMM lines was a glutathione S-transferase alpha 4 (*Gsta4*, Fig. 9). To confirm the expression of *Gsta4* in previous microarray analysis, we used qPCR analysis and found that IMM cells express higher *Gsta4* compared to the parental B16OVA cells (Fig. 10A). In addition, western blot analysis confirmed that the protein level of GSTA4 is higher in IMM cells in comparison to the parental B16OVA cells (Fig. 10B).

To examine the functional importance of *Gsta4* in IMM cells, we tested the cells with 4-hydroxynonenal (4-HNE), an oxidative lipid mainly catalyzed and detoxified by *Gsta4*. We discovered that IMM cell lines showed a relatively lower response to 4-HNE but not parental B16OVA cells or other variants (Fig. 11A). We further confirmed that all of the IMM cell lines established similarly responded to 4-HNE (Fig. 11B). These results indicate that immune-resistant melanoma variants specifically upregulated the expression of functional *Gsta4*.

3.4. Importance of *Gsta4* for restraining immune-resistant melanoma variants to IFN-γ-induced oxidative stress response

To investigate the functional role of *Gsta4* in protecting immune-resistant cancer cells from the IFN-γ-induced oxidative stress response, we established either B16OVA over-expressing *Gsta4* or IMM2 with knockdown of *Gsta4*. First, to establish the overexpressed cells, we subcloned the flag-tagged mouse *Gsta4* sequence into the pENTR1A vector. The m*Gsta4* and pENTR1A were amplified using polymerase chain reaction (PCR), and the product site was confirmed by electrophoresis (Fig. 12A). After assembling the flag-*Gsta4* into the pENTR1A vector, the plasmid was transformed, and the colonies were established the next day (P1 and P2). After purifying the DNA, the plasmid was enzymatically cut by restriction enzyme, PstI, and confirmed by gel electrophoresis (Fig. 12B). The plasmid sequences were read by sequencing, and the insert P2 was selected. The established pENTR1A_*Gsta4* fragment was subcloned into the pLenti CMV Hygro E2-Crimson vector and named pLCMVh_m*Gsta4*. The plasmid was transformed into *E. coli*, and after purifying the DNA, gel electrophoresis was performed to confirm the product by gel electrophoresis. From the results, pLCMVh_m*Gsta4* #2 was selected (Fig. 12C). The prepared pLCMVh_m*Gsta4* was transfected into Lenti-X 293T cells and infected to B16OVA cells on the following day and selected in puromycin. After the single-cell clones, we confirmed the overexpression of GSTA4 in B16OVA by checking the protein expression on western blot analysis, which was later named GSTA4 OE#1 and GSTA4 OE#2, respectively (Fig. 13).

Second, to establish the knockdown *Gsta4* cells, we use shRNA targeting mouse *Gsta4*. After the large culture of the plasmid in the LB medium and purifying the DNA, the plasmid was transfected into Lenti-X 293T cells and infected to IMM2 cells on the following day and selected in puromycin. We confirmed the knockdown of *Gsta4* in IMM2 by checking the mRNA level on qPCR analysis. The shGsta4 #31 and shGsta4 #34 showed the most decrease of *Gsta4* in IMM2 cells, later named IMM2-shGSTA4 #1 and IMM2-shGSTA4 #2, respectively (Fig. 14).

We found that GSTA4 OE#1 and GSTA4 OE#2 became resistant to the IFN-γ-induced cytostatic effect compared with the mock control cell B16OVA line (Fig. 15). Such resistance to IFN-γ partly corresponded to the reduction of ROS production (Fig. 16). In addition, IMM2-shGSTA4#1 and IMM2-shGSTA4#2 showed restored responsiveness to the IFN-γ-induced cytostatic effect similar to their parental B16OVA cells (Fig. 17). In response to IFN-γ, IMM2-shGSTA4#2 cells showed increased intracellular ROS levels (Fig. 18), similar to the parental B16OVA cells. Collectively, these results clearly indicate the critical involvement of GSTA4 in regulating the IFN-γ-induced oxidative stress response in melanoma cells.

3.5. *Gsta4* governs the immune-resistance ability of melanoma cells

To verify the relevance of *Gsta4* in IMM variants to evade the tumor-specific immune response by acquiring the resistance to the IFN-γ-induced oxidative stress response, we performed two different *in vivo* experiments using either *Gsta4* over-expressing cell line or *Gsta4* knockdown cell line. First, we

inoculated OVA-immunized mice B6 mice with parental B16OVA or B16OVA cells overexpressing *Gsta4* (GSTA4 OE#2) and monitored tumor growth. As shown in Figure 19, GSTA4 OE#2 cell growth was more aggressive than the parental B16OVA cells. Second, mice bearing IMM2 cells or IMM2-shGSTA4#2 cells were treated with anti-PD-1 to initiate tumor-specific immunity *in vivo*. In contrast to IMM2 cells, which exhibited no response (Fig. 20A), *Gsta4* knockdown in IMM2 cells regained the responsiveness to anti-PD-1 therapy *in vivo* (Fig. 20B). Given that there was no difference in T cell infiltration between IMM2-shCTRL and IMM2-shGSTA4 #2 tumors (Fig. 21A and B), these findings strongly suggest that *Gsta4* is the gene responsible for melanoma cells acquiring resistance to anti-tumor immunity.

3.6. Relevance of *GSTA4* expression in IFN-γ responsiveness of human melanoma

To evaluate the clinical relevance of our findings in murine melanoma cells, the response of three distinct human melanoma cell lines with particular *GSTA4* gene expression status to IFN-γ treatment was evaluated. According to the Cancer Cell Line Encyclopedia (45), mRNA expression of *GSTA4* was high, medium, and low in Malme3M, UACC 62, and MeWo, respectively. In addition to the expression of *GSTA4*, Malme3M was more resistant to IFN-γ treatment *in vitro* than the other two cell lines (Fig. 22). Importantly, melanoma patients with low *GSTA4* expression were better responders (Fig. 23A) and had better progression-free survival rate (Fig. 23B) to anti-PD-1 therapy (samples were taken pre-and on-treatment) (46,47). These results strongly

support the clinical relevance of our findings and suggest the importance of the *GSTA4* expression status in human melanoma in responsiveness to immunotherapy.

4. Discussion

In this study, we demonstrated that melanoma cells acquired resistance to IFN-γ-dependent host immunity by up-regulating *Gsta4* expression to manage cellular oxidative stress responses. Therefore, manipulation of the oxidative stress response in cancer cells may be a new therapeutic target to overcome immune-resistance. The glutathione S-transferases (GSTs) are a family of phase II detoxification enzymes that catalyze the conjugation of glutathione (GSH) to a variety of endogenous and exogenous electrophilic compounds, and play an important role in cellular oxidative stress responses (48). In cancer, GSTs are considered as therapeutic targets because specific isozymes of GSTs are overexpressed in various tumors, and also involved in regulating oncogenic signals and anti-cancer drug resistance (49). As with other GSTs, *Gsta4* is expressed in a variety of normal tissues, but its specific function is to catalyze the conjugation of reduced glutathione to 4-HNE (50); therefore, *Gsta4* protects cells from the oxidative stress response. During tumor development, the diverse mechanisms are often seen in cancer cells to escape from immune surveillance (51), and it is likely that management of the oxidative stress response by a cellular redox system may play a substantial role. In this context, a recent study reported that increased tumor cell lipid peroxidation by immunotherapy-activated CD8^{+} T cells led to tumor ferroptosis promoted by IFN-γ (28), suggesting the importance of the cellular redox system to regulate the tumor response to IFN-γ. Considering that *Gsta4* overexpression cannot fully protect B16OVA cells from the oxidative stress response induced by IFN-γ, *Gsta4* cannot be solely responsible for

protecting immune-escape variants from oxidative stress responses. In our gene expression analysis, we also identified the upregulation of AKR1B8 and NQO1 genes that are known to be involved in the cellular redox system (52,53), and those genes may have some redundant role in collaboration with *Gsta4* to fully protect immune-escape variants from IFN-γ-induced oxidative stress responses.

There are several limitation remains to clear in this study. Firstly, it is quite important to clarify whether those immune escape variants with high *Gsta4* expression were generated a result of selection of pre-existing population, or induced by a genetic evolution during immune-editing process. Although we could not directly answer to this question in this study, we previously reported the relevant findings that antigen-specific immunity by CTL and IFN-γ increases of genomic instability to immunoedit cancer cells for escaping from immunity (38). Therefore, we presume that the bearing high *Gsta4* expression in immune-escape variants should be a result of genetic modification during the immunoediting process. Secondary, our presented results are mostly concluded from different variants of B16 melanoma cell lines, and other human melanoma cell lines. Although the clinical relevance of our findings in human melanoma patients were shown, we could not conclude a general importance of *Gsta4* in immune-resistance of other cancer types. Nevertheless, our results suggest a novel mechanism whereby melanoma cells escape from host immunity by acquiring resistance to oxidative stress responses through the upregulation of *Gsta4*.

5. Conclusion

In this study, we demonstrated how to identify the immunological status of tumor antigen-specific CD8$^+$ T cells in the tumor microenvironment during tumor progression by developing a bioluminescence imaging model under different immunological conditions. Further, by using the generated model, we highlight a novel mechanism whereby cancer cells escape from host immunity by acquiring resistance to oxidative stress responses through the upregulation of *Gsta4*.

6. Reference

1. Mbeunkui F, Johann DJ. Cancer and the tumor microenvironment: a review of an essential relationship. Cancer Chemother Pharmacol. 2009;63(4):571–82.

2. Hanahan D, Weinberg RA. The Hallmarks of Cancer. Cell. 2000;100(1):57–70.

3. Hanahan D, Weinberg RA. Hallmarks of Cancer: The Next Generation. Cell. 2011;144(5):646–74.

4. Ehrlich P. Ueber den jetzigen Stand der Karzinomforschung. 1908.

5. Thomas L, Lawrence H. Cellular and humoral aspects of the hypersensitive states. N Y Hoeber-Harper. 1959;529–32.

6. Burnet M. Cancer--A Biological Approach: I. The Processes Of Control. II. The Significance of Somatic Mutation. BMJ. 1957;1(5022):779–86.

7. Shankaran V, Ikeda H, Bruce AT, White JM, Swanson PE, Old LJ, et al. IFNγ and lymphocytes prevent primary tumour development and shape tumour immunogenicity. Nature. 2001;410(6832):1107–11.

8. Dunn GP, Bruce AT, Ikeda H, Old LJ, Schreiber RD. Cancer immunoediting: from immunosurveillance to tumor escape. Nat Immunol. 2002;3(11):991–8.

9. Gao J, Shi LZ, Zhao H, Chen J, Xiong L, He Q, et al. Loss of IFN-γ Pathway Genes in Tumor Cells as a Mechanism of Resistance to Anti-CTLA-4 Therapy. Cell. 2016;167(2):397-404.e9.

10. Shin DS, Zaretsky JM, Escuin-Ordinas H, Garcia-Diaz A, Hu-Lieskovan S, Kalbasi A, et al. Primary Resistance to PD-1 Blockade Mediated by *JAK1/2* Mutations. Cancer Discov. 2017;7(2):188–201.

11. Platanias LC. Mechanisms of type-I- and type-II-interferon-mediated signalling. Nat Rev Immunol. 2005;5(5):375–86.

12. Schoenborn JR, Wilson CB. Regulation of interferon-gamma during innate and adaptive immune responses. Adv Immunol. 2007;96:41-101.

13. Ealick S, Cook W, Vijay-Kumar S, Carson M, Nagabhushan T, Trotta P, et al. Three-dimensional structure of recombinant human interferon-gamma. Science. 1991;252(5006):698–702.

14. Yeh TC, Pellegrini S. The Janus kinase family of protein tyrosine kinases and their role in signaling. Cell Mol Life Sci CMLS. 1999;55(12):1523–34.

15. Haan C, Kreis S, Margue C, Behrmann I. Jaks and cytokine receptors—An intimate relationship. Biochem Pharmacol. 2006;72(11):1538–46.

16. Brown TJ, Lioubin MN, Marquardt H. Purification and characterization of cytostatic lymphokines produced by activated human T lymphocytes. Synergistic antiproliferative activity of transforming growth factor beta 1,

interferon-gamma, and oncostatin M for human melanoma cells. J Immunol Baltim Md 1950. 1987;139(9):2977–83.

17. Dighe AS, Richards E, Old LJ, Schreiber RD. Enhanced in vivo growth and resistance to rejection of tumor cells expressing dominant negative IFNγ receptors. Immunity. 1994;1(6):447–56.

18. Kaplan DH, Shankaran V, Dighe AS, Stockert E, Aguet M, Old LJ, et al. Demonstration of an interferon γ-dependent tumor surveillance system in immunocompetent mice. Proc Natl Acad Sci. 1998;95(13):7556–61.

19. Weber JS, Rosenberg SA. Modulation of murine tumor major histocompatibility antigens by cytokines in vivo and in vitro. Cancer Res. 1988;48(20):5818–24.

20. Cornetta K, Berebitsky D, Behnia M, Traycoff C, Srour EF, Sledge GW. A retroviral vector expressing human interferon gamma upregulates MHC antigen expression in human breast cancer and leukemia cell lines. Cancer Gene Ther. 1994;1(2):91–8.

21. Street D, Kaufmann AM, Vaughan A, Fisher SG, Hunter M, Schreckenberger C, et al. Interferon-γ Enhances Susceptibility of Cervical Cancer Cells to Lysis by Tumor-Specific Cytotoxic T Cells. Gynecol Oncol. 1997;65(2):265–72.

22. Martini M, Testi MG, Pasetto M, Picchio MC, Innamorati G, Mazzocco M, et al. IFN-γ-mediated upmodulation of MHC class I expression activates tumor-

specific immune response in a mouse model of prostate cancer. Vaccine. 2010;28(20):3548–57.

23. Kochupurakkal BS, Wang ZC, Hua T, Culhane AC, Rodig SJ, Rajkovic-Molek K, et al. RelA-Induced Interferon Response Negatively Regulates Proliferation. PloS One. 2015;10(10):e0140243.

24. Wang L, Wang Y, Song Z, Chu J, Qu X. Deficiency of interferon-gamma or its receptor promotes colorectal cancer development. J Interferon Cytokine Res Off J Int Soc Interferon Cytokine Res. 2015;35(4):273–80.

25. Li W, Huang X, Tong H, Wang Y, Zhang T, Wang W, et al. Comparison of the regulation of β-catenin signaling by type I, type II and type III interferons in hepatocellular carcinoma cells. PloS One. 2012;7(10):e47040.

26. Wang QS, Shen SQ, Sun HW, Xing ZX, Yang HL. Interferon-gamma induces autophagy-associated apoptosis through induction of cPLA2-dependent mitochondrial ROS generation in colorectal cancer cells. Biochem Biophys Res Commun. 2018;498(4):1058–65.

27. Hubackova S, Kucerova A, Michlits G, Kyjacova L, Reinis M, Korolov O, et al. IFNγ induces oxidative stress, DNA damage and tumor cell senescence via TGFβ/SMAD signaling-dependent induction of Nox4 and suppression of ANT2. Oncogene. 2016;35(10):1236–49.

28. Wang W, Green M, Choi JE, Gijón M, Kennedy PD, Johnson JK, et al. CD8+ T cells regulate tumour ferroptosis during cancer immunotherapy. Nature. 2019;569(7755):270–4.

29. Müller-Hermelink N, Braumüller H, Pichler B, Wieder T, Mailhammer R, Schaak K, et al. TNFR1 Signaling and IFN-γ Signaling Determine whether T Cells Induce Tumor Dormancy or Promote Multistage Carcinogenesis. Cancer Cell. 2008;13(6):507–18.

30. Katz JB, Muller AJ, Prendergast GC. Indoleamine 2,3-dioxygenase in T-cell tolerance and tumoral immune escape. Immunol Rev. 2008;222(1):206–21.

31. Xiao M, Wang C, Zhang J, Li Z, Zhao X, Qin Z. IFNγ Promotes Papilloma Development by Up-regulating Th17-Associated Inflammation. Cancer Res. 2009;69(5):2010–7.

32. Zaidi MR, Davis S, Noonan FP, Graff-Cherry C, Hawley TS, Walker RL, et al. Interferon-γ links ultraviolet radiation to melanomagenesis in mice. Nature. 2011;469(7331):548–53.

33. Zou W, Wolchok JD, Chen L. PD-L1 (B7-H1) and PD-1 pathway blockade for cancer therapy: Mechanisms, response biomarkers, and combinations. Sci Transl Med. 2016;8(328):328rv4.

34. Bellucci R, Martin A, Bommarito D, Wang K, Hansen SH, Freeman GJ, et al. Interferon-γ-induced activation of JAK1 and JAK2 suppresses tumor cell

susceptibility to NK cells through upregulation of PD-L1 expression. Oncoimmunology. 2015;4(6):e1008824.

35. Algarra I, García-Lora A, Cabrera T, Ruiz-Cabello F, Garrido F. The selection of tumor variants with altered expression of classical and nonclassical MHC class I molecules: implications for tumor immune escape. Cancer Immunol Immunother CII. 2004;53(10):904–10.

36. Beatty GL, Paterson Y. IFN-γ Can Promote Tumor Evasion of the Immune System In Vivo by Down-Regulating Cellular Levels of an Endogenous Tumor Antigen. J Immunol. 2000;165(10):5502–8.

37. Morel S, Lévy F, Burlet-Schiltz O, Brasseur F, Probst-Kepper M, Peitrequin AL, et al. Processing of Some Antigens by the Standard Proteasome but Not by the Immunoproteasome Results in Poor Presentation by Dendritic Cells. Immunity. 2000;12(1):107–17.

38. Takeda K, Nakayama M, Hayakawa Y, Kojima Y, Ikeda H, Imai N, et al. IFN-γ is required for cytotoxic T cell-dependent cancer genome immunoediting. Nat Commun. 2017;8(1):14607.

39. Takahashi K, Nagai N, Ogura K, Tsuneyama K, Saiki I, Irimura T, et al. Mammary tissue microenvironment determines T cell-dependent breast cancer-associated inflammation. Cancer Sci. 2015;106(7):867–74.

40. Campeau E, Ruhl VE, Rodier F, Smith CL, Rahmberg BL, Fuss JO, et al. A Versatile Viral System for Expression and Depletion of Proteins in Mammalian Cells. PLOS ONE. 2009;4(8):e6529.

41. Xu X, Eshima S, Kato S, Fisher DE, Sakurai H, Hayakawa Y, et al. Rational Combination Therapy for Melanoma with Dinaciclib by Targeting BAK-Dependent Cell Death. Mol Cancer Ther. 2020;19(2):627–36.

42. Suzuki S, Zhou Y, Refaat A, Takasaki I, Koizumi K, Yamaoka S, et al. Human T Cell Lymphotropic Virus 1 Manipulates Interferon Regulatory Signals by Controlling the TAK1-IRF3 and IRF4 Pathways. J Biol Chem. 2010;285(7):4441–6.

43. Ogura K, Sato-Matsushita M, Yamamoto S, Hori T, Sasahara M, Iwakura Y, et al. NK Cells Control Tumor-Promoting Function of Neutrophils in Mice. Cancer Immunol Res. 2018;6(3):348–57.

44. Lin CF, Lin CM, Lee KY, Wu SY, Feng PH, Chen KY, et al. Escape from IFN-γ-dependent immunosurveillance in tumorigenesis. J Biomed Sci. 2017;24(1):10.

45. Barretina J, Caponigro G, Stransky N, Venkatesan K, Margolin AA, Kim S, et al. The Cancer Cell Line Encyclopedia enables predictive modelling of anticancer drug sensitivity. Nature. 2012;483(7391):603–7.

46. Tibor Fekete J, Győrffy B. A unified platform enabling biomarker ranking and validation for 1562 drugs using transcriptomic data of 1250 cancer cell lines. Comput Struct Biotechnol J. 2022;20:2885–94.

47. Lánczky A, Győrffy B. Web-Based Survival Analysis Tool Tailored for Medical Research (KMplot): Development and Implementation. J Med Internet Res. 2021;23(7):e27633.

48. Sheehan D, Meade G, Foley VM, Dowd CA. Structure, function and evolution of glutathione transferases: implications for classification of non-mammalian members of an ancient enzyme superfamily. Biochem J. 2001;360(Pt 1):1–16.

49. Townsend DM, Tew KD. The role of glutathione- S -transferase in anti-cancer drug resistance. Oncogene. 2003;22:7369–75.

50. Balogh LM, Atkins WM. Interactions of glutathione transferases with 4-hydroxynonenal. Drug Metab Rev. 2011;43(2):165–78.

51. Sharma P, Hu-Lieskovan S, Wargo JA, Ribas A. Primary, Adaptive, and Acquired Resistance to Cancer Immunotherapy. Cell. 2017;168(4):707–23.

52. Liu Y, Zhang J, Liu H, Guan G, Zhang T, Wang L, et al. Compensatory upregulation of aldo-keto reductase 1B10 to protect hepatocytes against oxidative stress during hepatocarcinogenesis. Am J Cancer Res. 2019;9(12):2730–48.

53. Ross D, Siegel D. Functions of NQO1 in Cellular Protection and CoQ10 Metabolism and its Potential Role as a Redox Sensitive Molecular Switch. Front Physiol. 2017;8:595.

7. Figure and legend
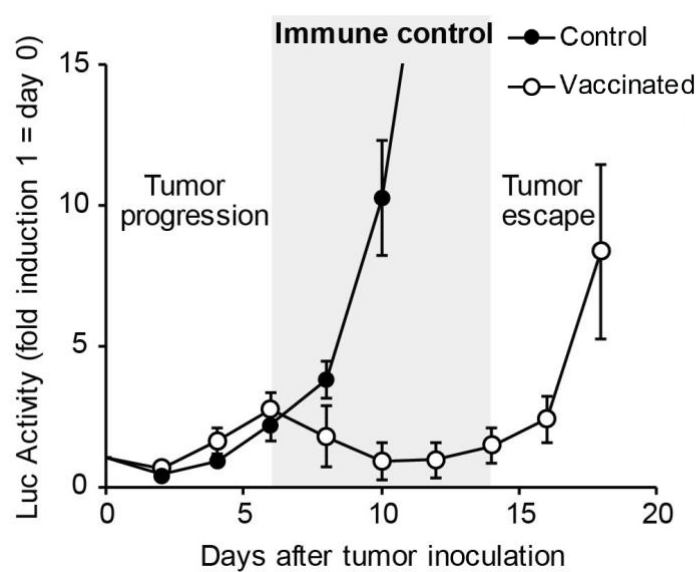
Figure 1. Identification of three phases of B16OVA-Luc2 growth in OVA-vaccinated mice

B16OVA-Luc2 cells were subcutaneously injected (10^5 cells/mouse) into untreated (Control) or OVA-vaccinated (Vaccinated) B6 mice, and the growth of B16OVA-Luc2 cells was monitored by bioluminescence imaging.
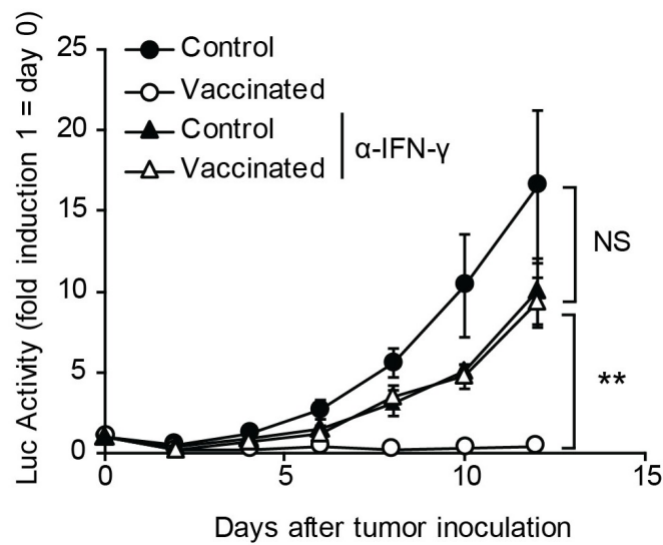
Figure 2. IFN-ɡ control B16OVA-Luc2 growth in OVA-vaccinated mice

B16OVA-Luc2 cells (10^5 cells/mouse) were subcutaneously implanted into into untreated (Control) or OVA-vaccinated (Vaccinated) B6 mice. To block IFN-ɡ, mice were treated with anti-IFN-ɡ (250 ∝g, i.p) every three days starting from day -1 (day 0 = tumor inoculation). Bioluminescence of the B16OVA-Luc2 tumor was monitored every other day and normalized by luminescence measured for an individual tumor on day 0. ** p<0.01, NS: not significant.
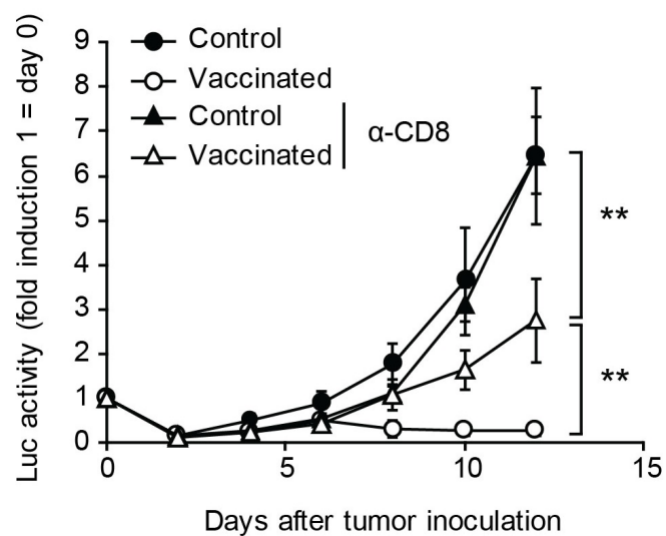
Figure 3. CD8⁺ T cells control B16OVA-Luc2 growth in OVA-vaccinated mice

B16OVA-Luc2 cells (10^5 cells/mouse) were subcutaneously implanted into into untreated (Control) or OVA-vaccinated (Vaccinated) B6 mice. To deplete CD8⁺ cells, mice were treated with anti-CD8 (250 mg, i.p) on days -3, -1, and 7 (day 0 = tumor inoculation). Bioluminescence of the B16OVA-Luc2 tumor was monitored every other day and normalized by luminescence measured for an individual tumor on day 0. ** p<0.01.
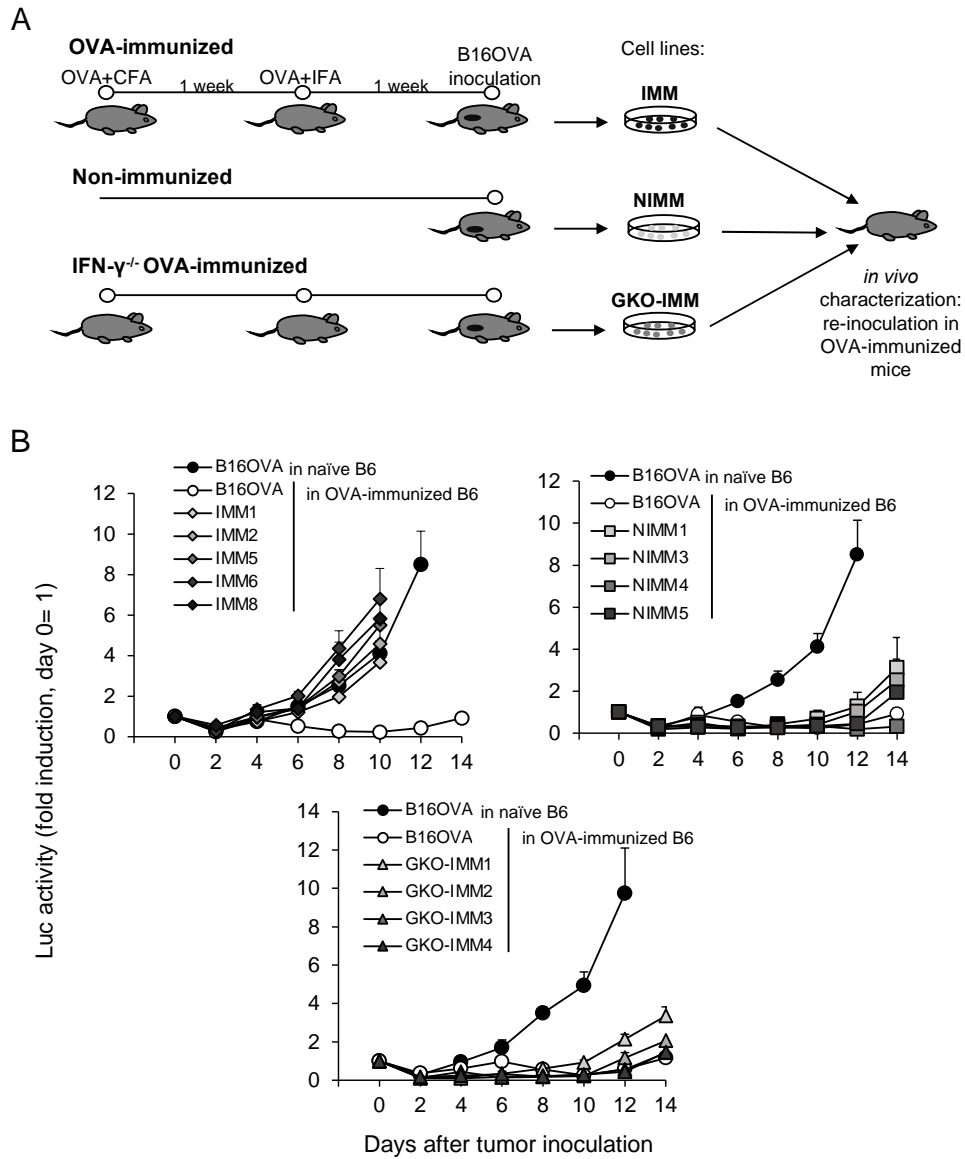
Figure 4. Establishment of immune-escape variants of B16OVA cells

Schematic illustration of the process to establish immune-escape variants, as well as other control variants, of B16OVA cells (A). Either naïve or OVA-immunized B6 mice were subcutaneously inoculated with the indicated cells (10^5 cells/mouse) and the growth of tumors was monitored by measuring the bioluminescence.
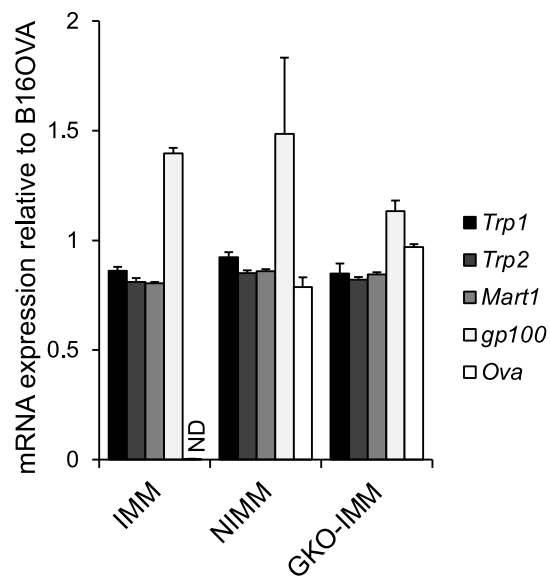
Figure 5. Antigen expression of immune-escape variants of B16OVA cells

Expression of melanoma antigen in the indicated cells was determined by RT-PCR.
ND: not detected.

A

B
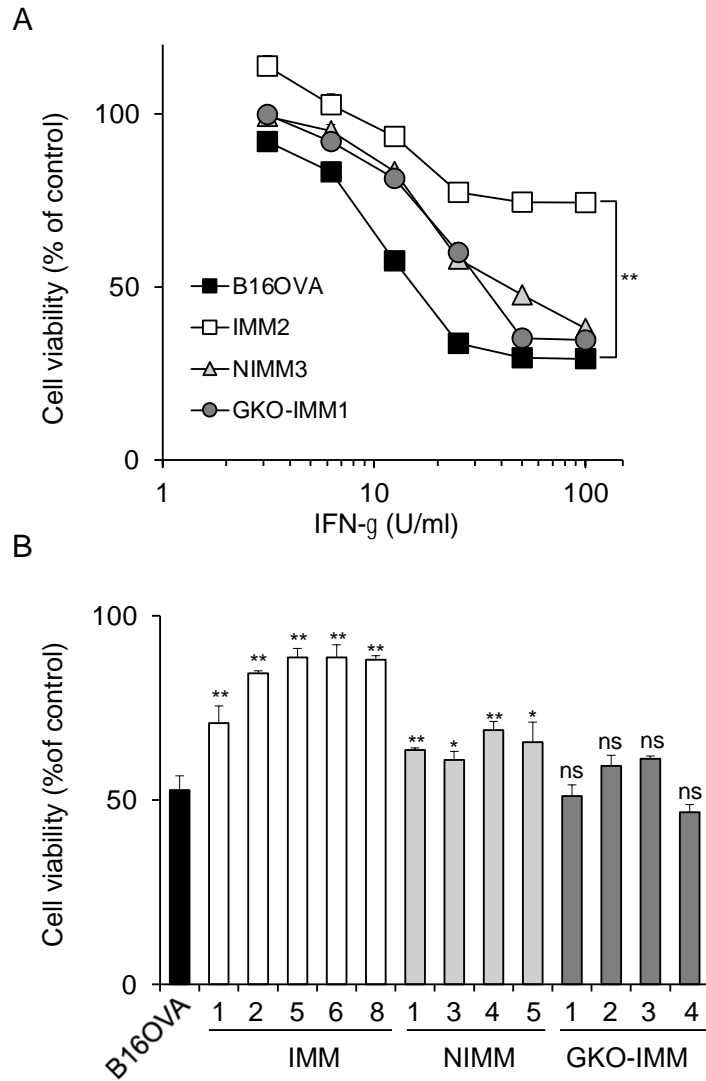
Figure 6. Resistance of immune-escape melanoma variants to IFN-g-induced cytostatic effect

The indicated cell lines were treated with different concentrations of IFN-g (A) or 20 U/mL of IFN-g (B) for 72 h. Cell viability (A, B, % of untreated control) was evaluated. Data are shown as mean $\pm$ SEM. ** p<0.01, * p<0.05, ns: not significant.
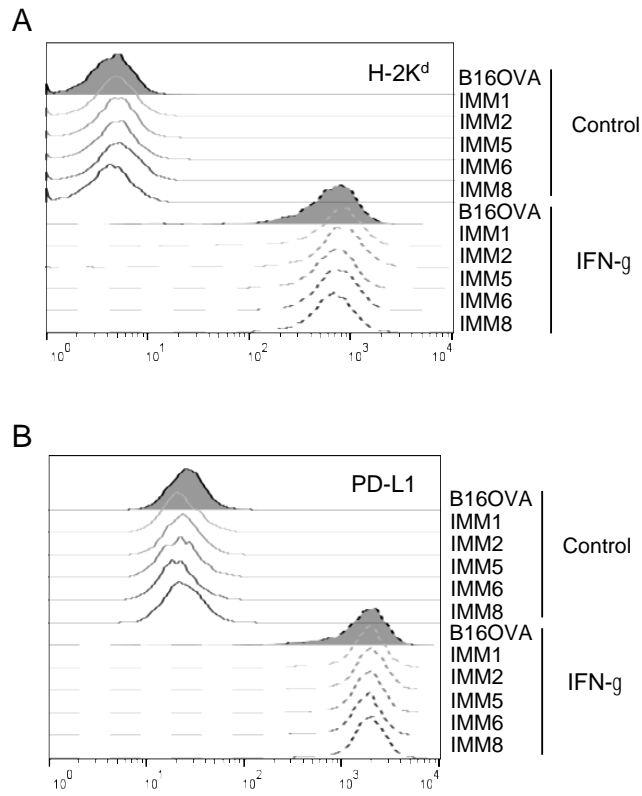
Figure 7. Responsiveness of immune-escape variants of B16OVA cells to IFN-g

The indicated cells were treated with or without IFN-g (20 U/mL) for 48 h, and the expression of H-2K^d MHC class I (A) or PD-L1 (B) was examined by flow cytometry.
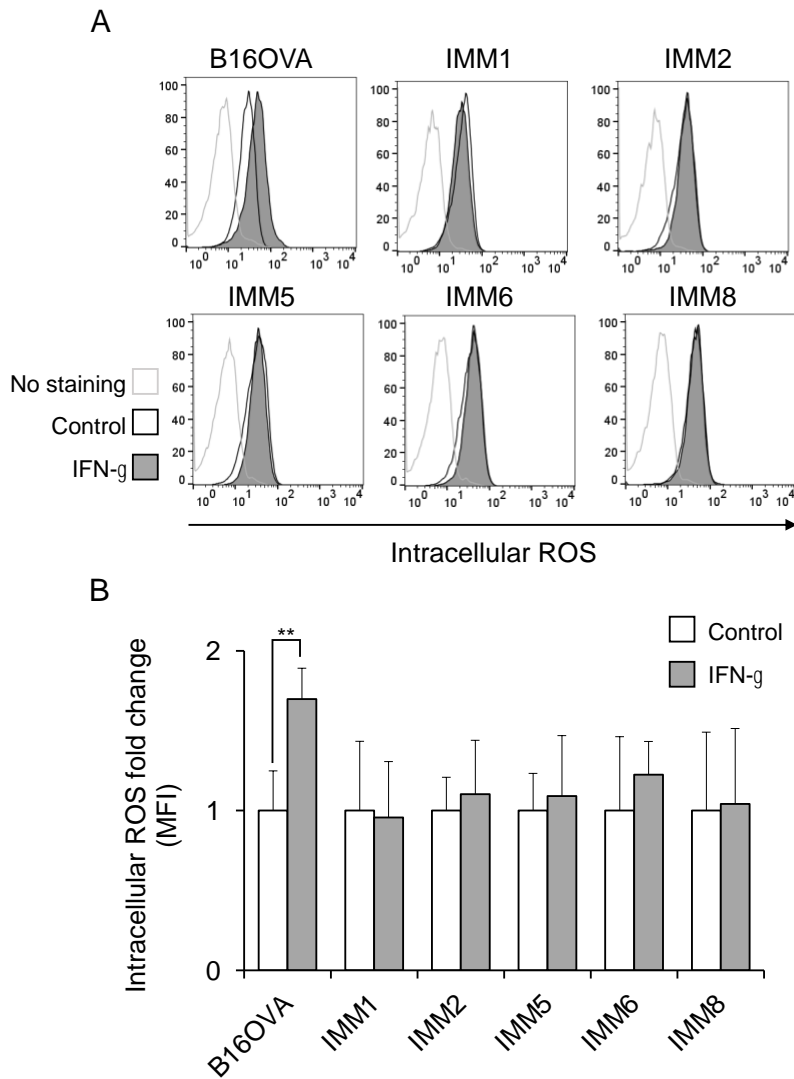
Figure 8. Unresponsiveness to IFN-g-induced intracellular ROS production in immune-escape variants of B16OVA cells

The indicated cell lines were treated with 20 U/mL of IFN-g for 72 h. The intracellular ROS expression (A. histogram, B. fold change to untreated control of mean fluorescent intensity) are shown. Data are shown as mean $\pm$ SEM. ** $p<0.01$.
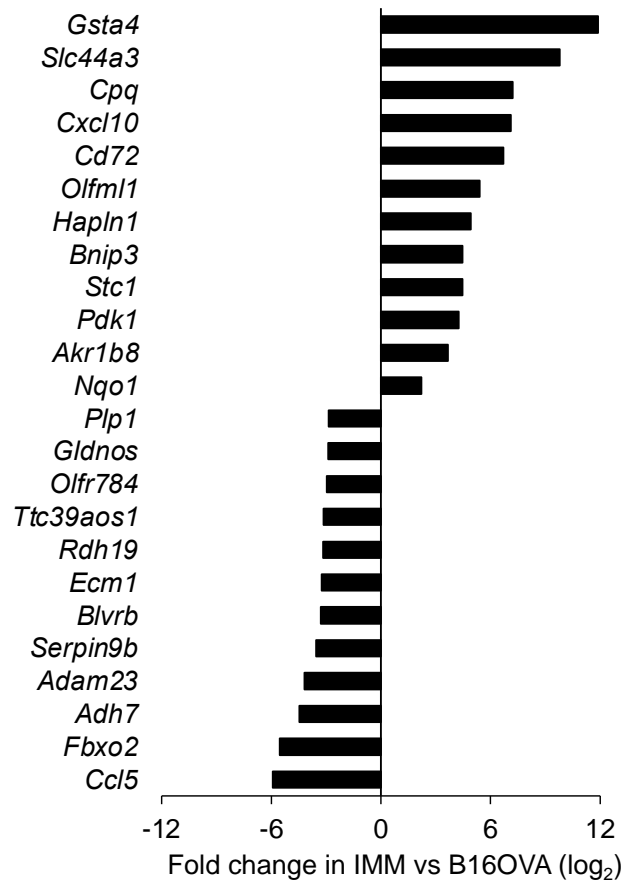
Figure 9. Differential gene expression status of immune-resistant B16 melanoma variants

The top 10 genes up- and downregulated in immune-resistant melanoma variants (IMM) compared with parental B16OVA are listed.
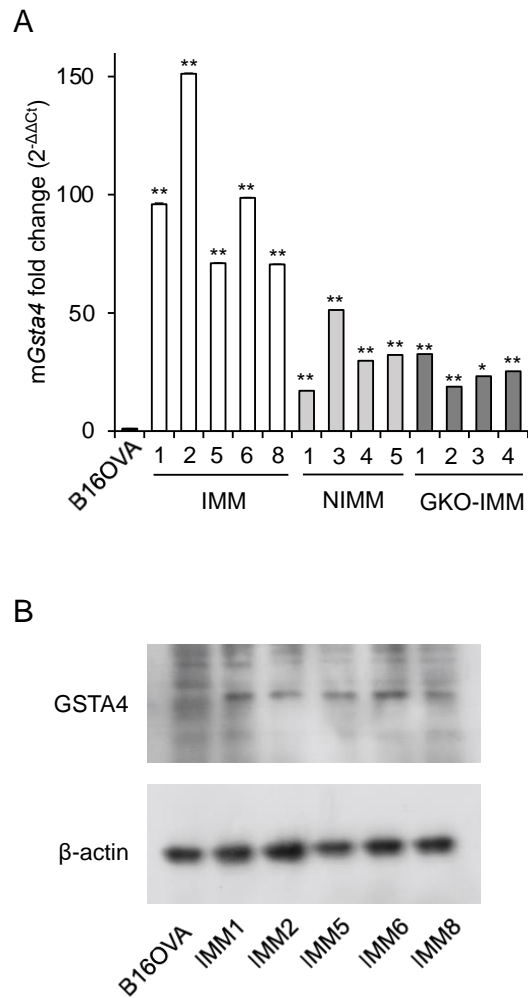
Figure 10. Functional upregulation of GSTA4 in immune-resistant melanoma variants

(A) Relative mRNA expression (fold change, B16OVA =1) and (B) protein expression of GSTA4 in the indicated cell lines are shown. Data are shown as mean $\pm$ SEM. ** p<0.01, * p<0.05.

A

B
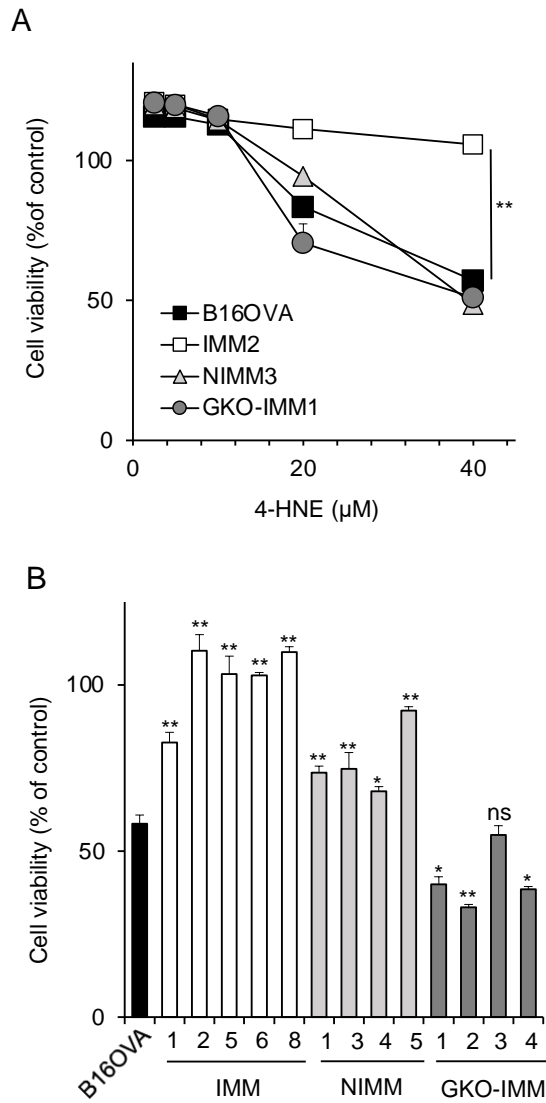
Figure 11. Unresponsiveness of immune-resistant melanoma variants to 4-HNE

The indicated cell lines treated with different concentrations of 4-HNE (A) or 40 μM of 4-HNE (B) for 24 h and cell viability were evaluated as relative to the untreated control. Data are shown as mean $\pm$ SEM. ** $p<0.01$, * $p<0.05$.
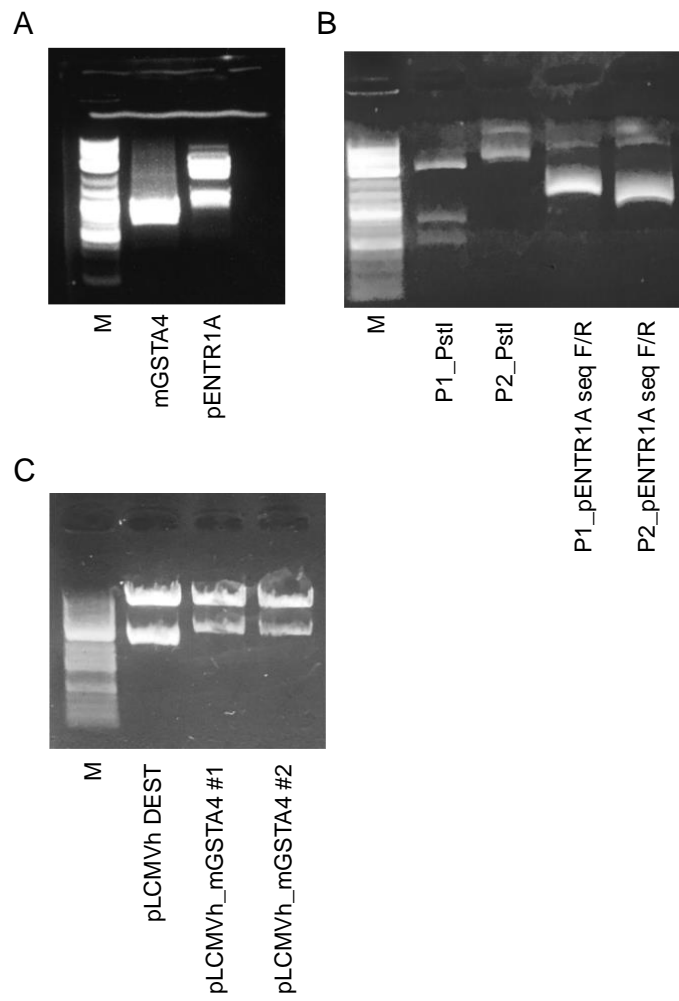
Figure 12. Establishment of the expression plasmid for *Gsta4* gene

The product site of m*GSTA4* and pENTR1A (A), P1_pENTR1A seq F/R and P2_pENTR1A seq F/R (B), and pLCMVh_mGSTA4 #1 and pLCMVh_mGSTA4 #2 (C) was confirmed by gel electrophoresis. M: Molecular weight marker.
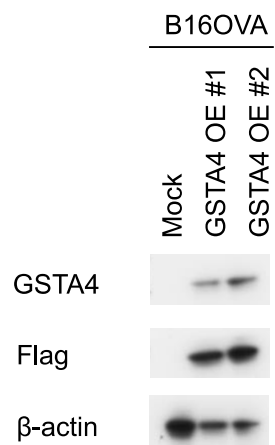
Figure 13. Establishment of GSTA4 over-expressing B16OVA cells

Expression of GSTA4 in the indicated cells was determined by Western blotting..
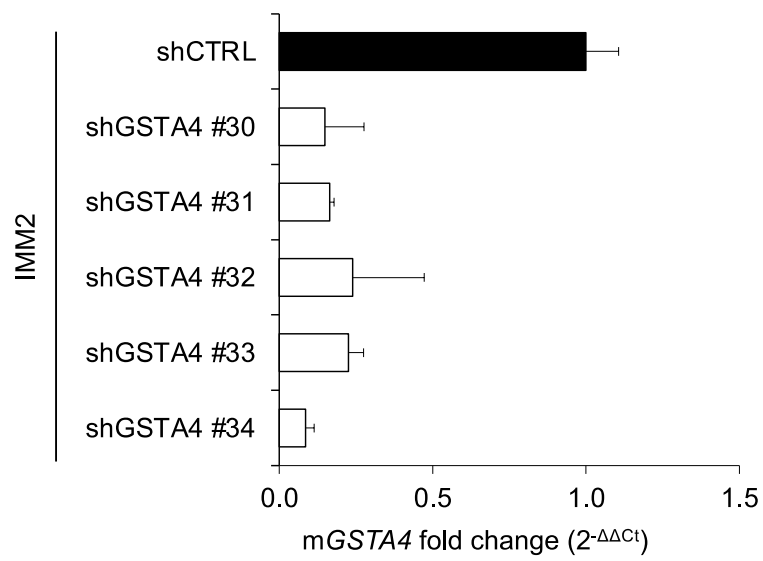
Figure 14. Establishment of *Gsta4* knock-down IMM2 cells

Expression of *Gsta4* in the indicated cells was determined by RT-PCR.
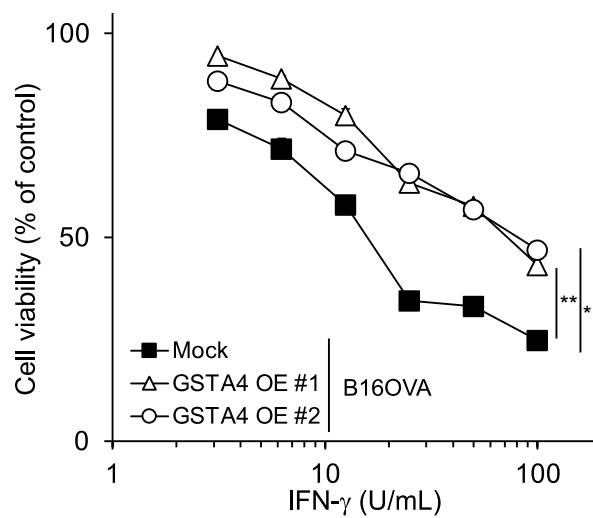
Figure 15. Effect of _Gsta4_ overexpression in B16OVA cells against IFN-γ-induced cytostatic effect

Control (Mock) or _Gsta4_ over-expressing (GSTA4 OE #1 and GSTA4 OE #2) B16OVA cell lines were treated with the indicated concentrations of IFN-γ for 72 h, and then the cell viability were determined. Data are shown as mean ± SEM. ** p<0.01, * p<0.05.
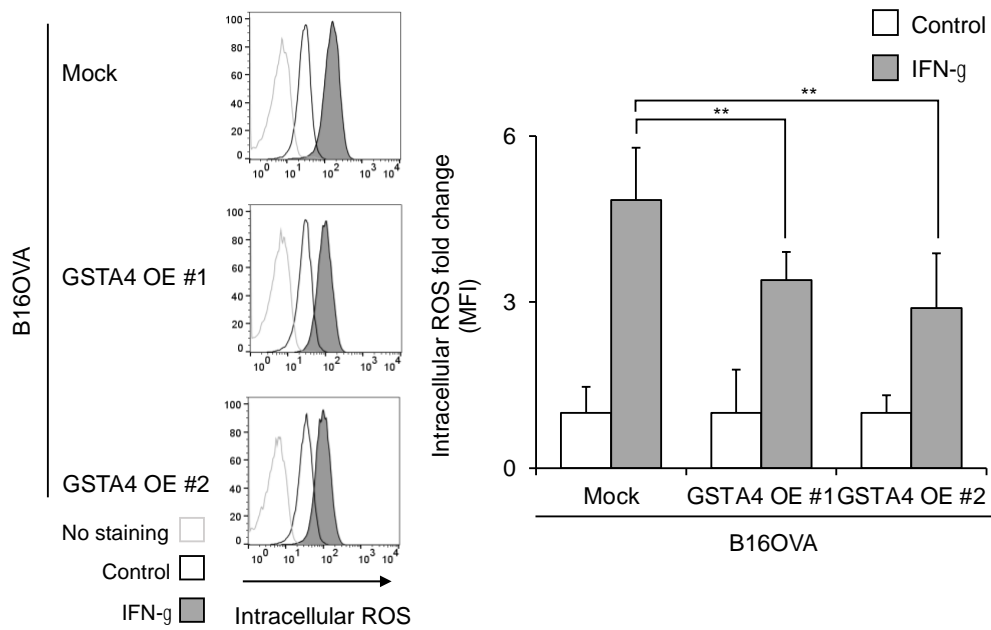
Figure 16. Effect of *Gsta4* overexpression in B16OVA cells against IFN-g-induced intracellular ROS production

Control (Mock) or *Gsta4* over-expressing (GSTA4 OE #1 and GSTA4 OE #2) B16OVA cell lines were treated with the indicated concentrations of IFN-g for 72 h, and then the intracellular ROS level were determined. Data are shown as mean $\pm$ SEM. ** $p<0.01$.
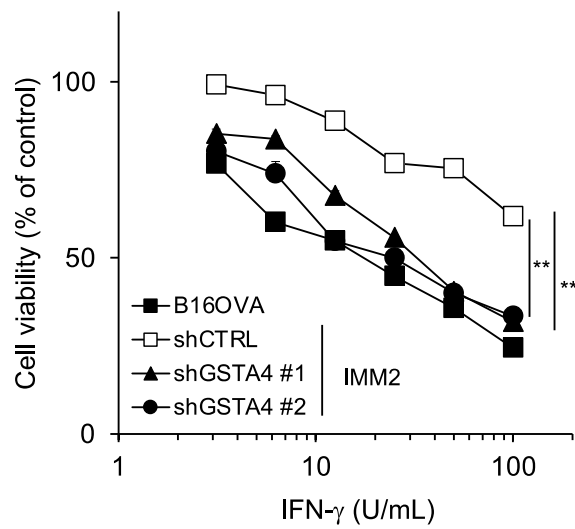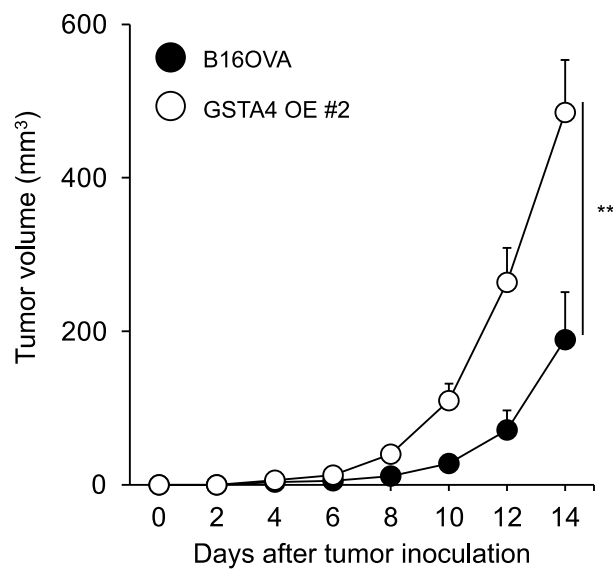
Figure 17. Involvement of *Gsta4* in the resistance of IMM2 cells against IFN-γ-induced cytostatic effect

IMM2 cells transduced with control shRNA (shCTRL) or *Gsta4* shRNA (shGSTA4 #1 and shGSTA4 #2) were treated with the indicated concentrations of IFN-γ for 72 h, and then the cell viability were determined. Data are shown as mean $\pm$ SEM. ** p<0.01.
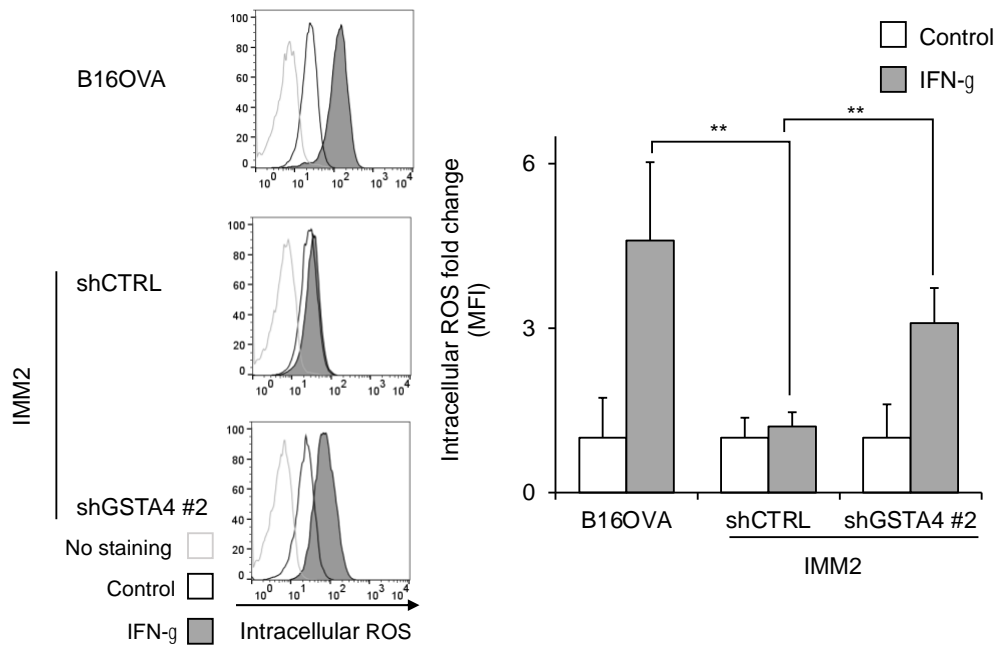
Figure 18. Involvement of *Gsta4* in the resistance of IMM2 cells against IFN-ɡ-induced intracellular ROS production

IMM2 cells transduced with control shRNA (shCTRL) or *Gsta4* shRNA (shGSTA4 #1 and shGSTA4 #2) were treated with the indicated concentrations of IFN-ɡ for 72 h, and then the intracellular ROS level were determined. Data are shown as mean $\pm$ SEM. ** p<0.01.

Figure 19. *Gsta4*-overexpression reduces the in vivo growth of B16OVA cells in OVA-immunized mice

OVA-immunized mice were subcutaneously injected (10^5 cells/mouse) with B16OVA or GSTA4 OE #2 cells. Tumor volumes were measured by calipers and the data are shown as mean $\pm$ SEM. ** $p < 0.01$.
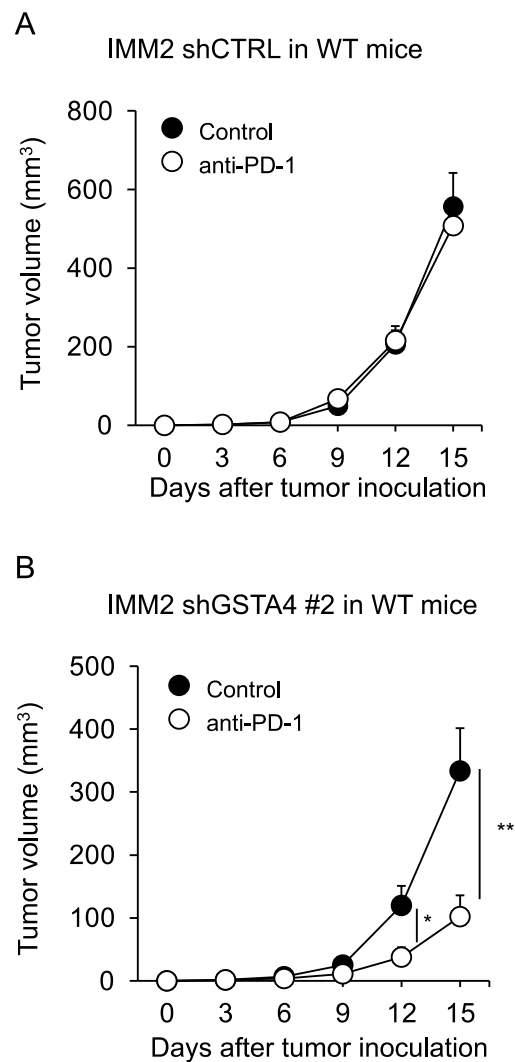
Figure 20. *Gsta4* knockdown in IMMs cells reinvigorates the responsiveness to anti-PD-1 blocking antibody in vivo

WT B6 mice were subcutaneously injected (10^5 cells/mouse) with IMM2 shCTRL cells (A) or IMM2 shGSTA4 #2 cells (B), and treated with saline (Control) or anti-PD-1 mAb (anti-PD-1, 250 μg/mouse) on days 3, 6, and 9 after the injection. Tumor volumes were measured by calipers and the data are shown as mean ± SEM. ** $p<0.01$.
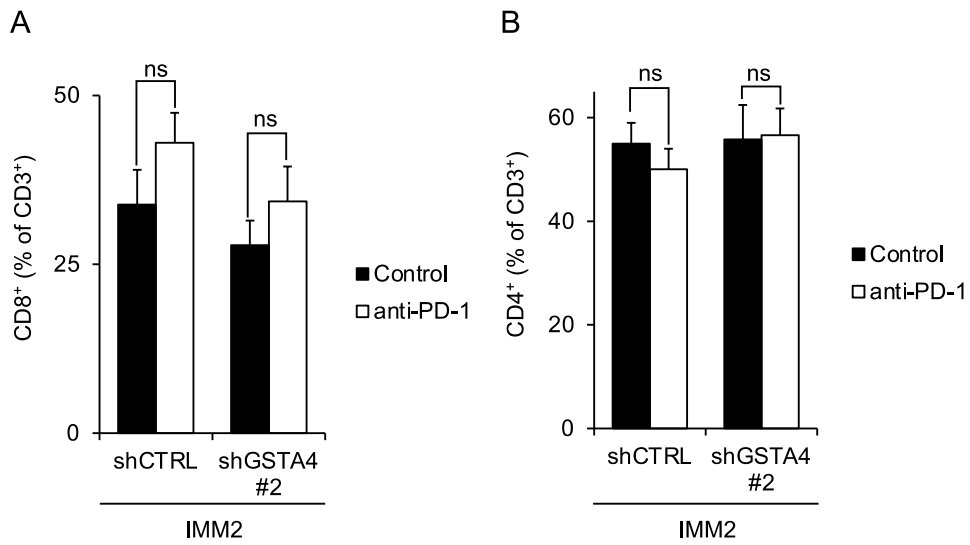
Figure 21. Tumor-infiltrating T cell status in IMM2 shCTRL and IMM2 shGSTA4 tumors

WT mice were subcutaneously injected (10^5 cells/mouse) with IMM2 shCTRL cells or IMM2 shGSTA4 #2 cells and treated with saline (Control) or anti-PD-1 mAb (anti-PD-1, 250 µg/mouse) on days 3, 6, and 9 after the injection. After 14 days of transplantation, tumors samples were collected and subjected to flow cytometry analysis of CD8+ (A) and CD4+ (B) T cell population. Data are shown as mean ± SEM. ns: not significant.
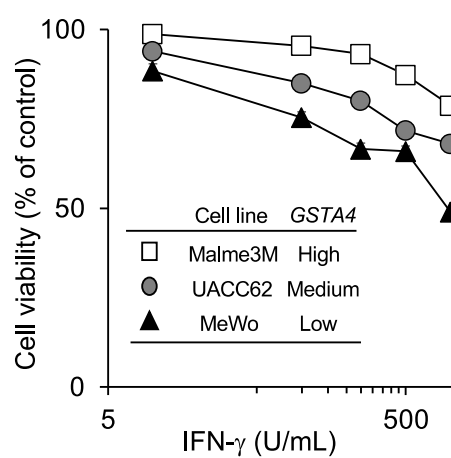
Figure 22. Responsiveness of human melanoma with different *GSTA4* expression status to IFN-γ-induced cytostatic effect

Human melanoma cell lines (Malme3M, UACC62, and MeWo) with different *GSTA4* expression levels (according to Cancer Cell Line Encyclopedia) were treated with the indicated concentrations of IFN-γ for 72 h, and then cell viability was evaluated. Data are shown as the mean ± SEM.
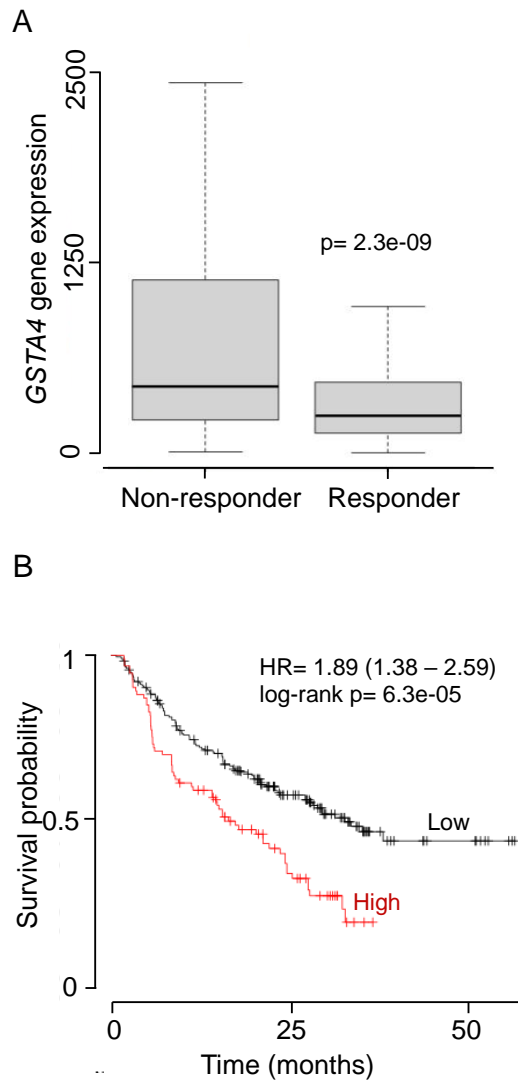
A

GSTA4 gene expression

p= 2.3e-09

Non-responder   Responder

B

Survival probability

HR= 1.89 (1.38 – 2.59)
log-rank p= 6.3e-05

Low

High

Time (months)

Figure 23. Relevance of *GSTA4* expression in the responsiveness and survival probability of anti-PD-1 treatment in human melanoma patients

(A) *GSTA4* expression related to the respond of anti-PD-1 treatment of melanoma patients generated by ROC plotter database is shown. (B) Kaplan Meier survival plot of melanoma patients treated with anti-PD-1 treatment related to the high or low *GSTA4* expression generated by KM plotter database is shown.

Acknowledgments

I want to express my appreciation and deep gratitude to people who, in one way or another, have contributed to making this study possible and my working experience valuable.

First and foremost, my deepest gratitude to Professor Yoshihiro Hayakawa for giving me countless opportunities to discover and grow. I am grateful to learn from how you think and your fantastic idea. I appreciate your patience, always being available and supportive, and never stopping my enthusiasm for science. It has been such incredible years to be able to join your padawan training.

I want to thank Associate Professor Satoru Yokoyama for being one of the people who taught me good science since day one in Toyama. Thank you for helping on the GSTA4 project and always being there when I needed some guidance.

My greatest appreciation to Dr. Marija Mojic for being a good role model, for the great discussion and idea, and for being one of the people who made me grow. Working on such an inspiring project with you has been a remarkable personal and scientific experience.

A warm gratitude to Professor Hiroaki Sakurai and Professor Takanori So for being the referee of my thesis. Thank you for the effort to review the thesis and for the thoughtful comments that ensued.

A deep thanks to Oki Kohei, Ohshima Chikako, and Haruka Tsuihiji for the excellent teamwork and valuable results on the GSTA4 project.

Thanks to Assistant Professor Takeshi Susukida and Assistant Professor So-ichiro Sasaki for having that critical mind that improved the project and presentation.